Satellite remote sensing reveals regional tropospheric aerosol trends

Michael I. Mishchenko[1*] and Igor V. Geogdzhayev[2]

[1]NASA Goddard Institute for Space Studies, 2880 Broadway, New York, NY 10025
[2]Columbia University and NASA Goddard Institute for Space Studies, 2880 Broadway, New York, NY 10025
[*]*mmishchenko@giss.nasa.gov*

Abstract: The Global Aerosol Climatology Project data product based on analyses of channel 1 and 2 AVHRR radiances shows significant regional changes in the retrieved optical thickness of tropospheric aerosols which had occurred between the volcano-free periods 1988–91 and 2002–05. These trends appear to be generally plausible, are consistent with extensive sets of long-term ground-based observations throughout the world, and may increase the trustworthiness of the recently identified downward trend in the global tropospheric aerosol load.

©2007 Optical Society of America

OCIS codes: (010.1100) Aerosol detection; (010.1110) Aerosols; (010.1310) Atmospheric scattering; (010.7030) Troposphere.

References and links

1. P. Chýlek and J. Coakley, "Aerosols and climate," Science **183**, 75–77 (1974).
2. V. Ramanathan, P. J. Crutzen, J. T. Kiehl, and D. Rosenfeld, "Aerosols, climate, and the hydrological cycle," Science **294**, 2119 – 2124 (2001).
3. S. E. Schwartz, "Uncertainty requirements in radiative forcing of climate change," J. Air Waste Manage. Assoc. **54**, 1351–1359 (2004).
4. J. E. Penner, S. Y. Zhang, M. Chin, C. C. Chuang, J. Feichter, Y. Feng, I. V. Geogdzhayev, P. Ginoux, M. Herzog, A. Higurashi, D. Koch, C. Land, U. Lohmann, M. Mishchenko, T. Nakajima, G. Pitari, B. Soden, I. Tegen, and L. Stowe, "A comparison of model- and satellite-derived aerosol optical depth and reflectivity," J. Atmos. Sci. **59**, 441–460 (2002).
5. M. I. Mishchenko, B. Cairns, J. E. Hansen, L. D. Travis, R. Burg, Y. J. Kaufman, J. V. Martins, and E. P. Shettle, "Monitoring of aerosol forcing of climate from space: analysis of measurement requirements," J. Quant. Spectrosc. Radiat. Transfer **88**, 149–161 (2004).
6. G. Myhre, N. Bellouin, T. F. Berglen, T. K. Berntsen, O. Boucher, A. Grini, I. S. A. Isaksen, M. Johnsrud, M. I. Mishchenko, F. Stordal, and D. Tanré, "Comparison of the radiative properties and direct radiative effect of aerosols from a global aerosol model and remote sensing data over ocean," Tellus B **59**, 115–129 (2007).
7. P. Goloub, D. Tanré, J. L. Deusé, M. Herman, A. Marchand, and F.-M. Bréon, "Validation of the first algorithm applied for deriving the aerosol properties over the ocean using the POLDER/ADEOS measurements," IEEE Trans. Geosci. Remote Sens. 37, 1586–1596 (1999).
8. M. I. Mishchenko, I. V. Geogdzhayev, B. Cairns, W. B. Rossow, and A. A. Lacis, "Aerosol retrievals over the ocean by use of channels 1 and 2 AVHRR data: sensitivity analysis and preliminary results," Appl. Opt. **38**, 7325–7341 (1999).
9. M. Wang, S. Bailey, C. R. McClain, "SeaWiFS provides unique global aerosol optical property data," EOS Trans. Amer. Geophys. Union **81**, 197 (2000).
10. O. Torres, P. K. Bhartia, J. R. Herman, A. Sinyuk, P. Ginoux, and B. Holben, "A long-term record of aerosol optical depth from TOMS observations and comparison to AERONET measurements," J. Atmos. Sci. **59**, 398–413 (2002).
11. A. Ignatov and N. R. Nalli, "Aerosol retrievals from multi-year multi-satellite AVHRR Pathfinder Atmosphere (PATMOS) dataset for correcting remotely sensed sea surface temperatures," J. Atmos. Oceanic Technol. **19**, 1986–2008 (2002).
12. P. Chýlek, B. Henderson, and M. Mishchenko, "Satellite based retrieval of aerosol optical thickness: the effect of sun and satellite geometry," Geophys. Res. Lett. **30**, 1533 (2003).
13. L. R. Poole, D. M. Winker, J. R. Pelon, and M. P. McCormick, "CALIPSO: global aerosol and cloud observations from lidar and passive instruments," Proc. SPIE **4881**, 419–426 (2003).
14. R. A. Kahn, B. J. Gaitley, J. V. Martonchik, D. J. Diner, K. A. Crean, and B. Holben, "Multiangle Imaging Spectroradiometer (MISR) global aerosol optical depth validation based on 2 years of coincident Aerosol

Robotic Network (AERONET) observations," J. Geophys. Res. **110**, D10S04 (2005).

15. L. A. Remer, Y. F. Kaufman, D. Tanré, S. Mattoo, D. A. Chu, J. V. Martins, R.-R. Li, C. Ichoku, R. C. Levy, R. G. Kleidman, T. F. Eck, E. Vermote, and B. N. Holben, "The MODIS aerosol algorithm, products and validation," J. Atmos. Sci. **62**, 947–973 (2005).
16. C. Pierangelo, M. Mishchenko, Y. Balkanski, and A. Chédin, "Retrieving the effective radius of Saharan dust coarse mode from AIRS," Geophys. Res. Lett. **32**, L20813 (2005).
17. E. Carboni, "GOME aerosol optical depth retrieval over ocean: correcting for the effects of residual cloud contamination," Atmos. Environ. **40**, 6975–6987 (2006).
18. M. I. Mishchenko, I. V. Geogdzhayev, B. Cairns, B. E. Carlson, J. Chowdhary, A. A. Lacis, L. Liu, W. B. Rossow, and L. D. Travis, "Past, present, and future of global aerosol climatologies derived from satellite observations: a perspective," J. Quant. Spectrosc. Radiat. Transfer **106**, 325–347 (2007).
19. M. I. Mishchenko, I. V. Geogdzhayev, W. B. Rossow, B. Cairns, B. E. Carlson, A. A. Lacis, L. Liu, and L. D. Travis, "Long-term satellite record reveals likely recent aerosol trend," Science **315**, 1543 (2007).
20. I. V. Geogdzhayev, M. I. Mishchenko, W. B. Rossow, B. Cairns, and A. A. Lacis, "Global two-channel AVHRR retrievals of aerosol properties over the ocean for the period of NOAA-9 observations and preliminary retrievals using NOAA-7 and NOAA-11 data," J. Atmos. Sci. **59**, 262–278 (2002).
21. M. I. Mishchenko, I. V. Geogdzhayev, L. Liu, J. A. Ogren, A. A. Lacis, W. B. Rossow, J. W. Hovenier, H. Volten, and O. Muñoz, "Aerosol retrievals from AVHRR radiances: effects of particle nonsphericity and absorption and an updated long-term global climatology of aerosol properties," J. Quant. Spectrosc. Radiat. Transfer **79/80**, 953–972 (2003).
22. I. V. Geogdzhayev, M. I. Mishchenko, L. Liu, and L. Remer, "Global two-channel AVHRR aerosol climatology: effects of stratospheric aerosols and preliminary comparisons with MODIS and MISR retrievals," J. Quant. Spectrosc. Radiat. Transfer **88**, 47–59 (2004).
23. I. V. Geogdzhayev, M. I. Mishchenko, E. I. Terez, G. A. Terez, and G. K. Gushchin, "Regional advanced very high resolution radiometer-derived climatology of aerosol optical thickness and size," J. Geophys. Res. **110**, D23205 (2005).
24. Global Aerosol Climatology Project. http://gacp.giss.nasa.gov.
25. M. Wild, H. Gilgen, A. Roesch, A. Ohmura, C. N. Long, E. G. Dutton, B. Forgan, A. Kallis, V. Russak, and A. Tsvetkov, "From dimming to brightening: decadal changes in solar radiation at Earth's surface," Science **308**, 847–850 (2005).
26. R. T. Pinker, B. Zhang, and E. G. Dutton, "Do satellites detect trends in surface solar radiation?" Science **308**, 850–854 (2005).
27. A. Ohmura, "Observed long-term variations of solar irradiance at the Earth's surface," Space Sci. Rev. **125**, 111–128 (2006).
28. M. Wild, A. Ohmura, and K. Makowski, "Impact of global dimming and brightening on global warming," Geophys. Res. Lett. **34**, L04702 (2007).
29. G. Stanhill, "A perspective on global warming, dimming, and brightening," EOS Trans. Amer. Geophys. Union **88**, 58 (2007).
30. J. Hansen, M. Sato, R. Ruedy, K. Lo, D. W. Lea, and M. Medina-Elizade, "Global temperature change," Proc. Natl. Acad. Sci. USA **103**, 14288–14293 (2006).
31. International Satellite Cloud Climatology Project. http://isccp.giss.nasa.gov.
32. W. B. Rossow and R. A. Schiffer, "Advances in understanding clouds from ISCCP," Bull. Amer. Meteorol. Soc. **80**, 2261–2287 (1999).
33. C. L. Brest, W. B. Rossow, and M. D. Roiter, "Update of radiance calibration for ISCCP," J. Atmos. Oceanic Technol. **14**, 1091–1109 (1997).
34. A. Ignatov, I. Laszlo, E. D. Harrod, K. B. Kidwell, and G. P. Goodrum, "Equator crossing times for NOAA, ERS and EOS sun-synchronous satellites," Int. J. Remote Sens. **25**, 5255–5266 (2004).
35. M. I. Mishchenko, L. D. Travis, and A. A. Lacis, *Scattering, Absorption, and Emission of Light by Small Particles* (Cambridge U. Press, Cambridge, UK, 2002). http://www.giss.nasa.gov/~crmim/books.html.
36. J. E. Hansen and L. D. Travis, "Light scattering in planetary atmospheres," Space Sci. Rev. **16**, 527–610 (1974).
37. M. I. Mishchenko and L. D. Travis, "Satellite retrieval of aerosol properties over the ocean using polarization as well as intensity of reflected sunlight," J. Geophys. Res. **102**, 16989–17013 (1997). http://www.giss.nasa.gov/~crmim/brf.
38. A. A. Lacis and V. Oinas, "A description of the correlated k-distribution method for modeling non-grey gaseous absorption, thermal emission, and multiple scattering in vertically inhomogeneous atmospheres," J. Geophys. Res. **96**, 9027–9063 (1991).
39. L. Liu and M. I. Mishchenko, "Effects of aggregation on scattering and radiative properties of soot aerosols," J. Geophys. Res. **110**, D11211 (2005).
40. O. Dubovik, A. Sinyuk, T. Lapyonok, B. N. Holben, M. Mishchenko, P. Yang, T. F. Eck, H. Volten, O. Muñoz, B. Veihelmann, W. J. van der Zande, J.-F. Leon, M. Sorokin, and I. Slursker, "Application of spheroid models to account for aerosol particle nonsphericity in remote sensing of desert dust," J. Geophys. Res. **111**, D11208 (2006).
41. Y. Zhang, W. B. Rossow, A. A. Lacis, V. Oinas, and M. I. Mishchenko, "Calculation of radiation fluxes from the surface to top of atmosphere based on ISCCP and other global data sets: refinements of the radiative transfer model and the input data," J. Geophys. Res. **109**, D19105 (2004).

42. L. Liu, M. I. Mishchenko, I. Geogdzhayev, A. Smirnov, S. M. Sakerin, D. M. Kabanov, and O. A. Ershov, "Global validation of two-channel AVHRR aerosol optical thickness retrievals over the oceans," J. Quant. Spectrosc. Radiat. Transfer **88**, 97–109 (2004).

43. A. Smirnov, B. N. Holben, S. M. Sakerin, D. M. Kabanov, I. Slutsker, M. Chin, T. L. Diehl, L. A. Remer, R. Kahn, A. Ignatov, L. Liu, M. Mishchenko, T. F. Eck, T. L. Kucsera, D. Giles, and O. V. Kopelevich, "Ship-based aerosol optical depth measurements in the Atlantic Ocean: comparison with satellite retrievals and GOCART model," Geophys. Res. Lett. **33**, L14817 (2006).

44. L. Olsson, L. Eklundh, and J. Ardö, "A recent greening of the Sahel—trends, patterns and potential causes," J. Arid Environ. **63**, 556–566 (2005).

45. S. M. Herrmann, A. Anyamba, and C. J. Tucker, "Recent trends in vegetation dynamics in the African Sahel and their relationship to climate," Global Environ. Change **15**, 394–404 (2005).

46. D. I. Stern, "Reversal of the trend in global anthropogenic sulfur emissions," Global Environ. Change **16**, 207–220 (2006).

47. D. G. Streets, Y. Wu, and M. Chin, "Two-decadal aerosol trends as a likely explanation of the global dimming/brightening transition," Geophys. Res. Lett. **33**, L15806 (2006).

48. T. Ohara, H. Akimoto, J. Kurokawa, N. Horii, K. Yamaji, X. Yan, and T. Hayasaka, "An Asian emission inventory of anthropogenic emission sources for the period 1980–2020," Atmos. Chem. Phys. Discuss. **7**, 6843–6902 (2007).

49. Special Sensor Microwave/Imager Project. http://www.remss.com.

50. E. R. Lewis and S. E. Schwartz, *Sea Salt Aerosol Production* (American Geophysical Union, Washington, DC, 2004).

51. M. I. Mishchenko, B. Cairns, G. Kopp, C. F. Schueler, B. A. Fafaul, J. E. Hansen, R. J. Hooker, T. Itchkawich, H. B. Maring, and L. D. Travis, "Accurate monitoring of terrestrial aerosols and total solar irradiance: introducing the Glory mission," Bull. Amer. Meteorol. Soc. **88**, No. 5, in press (2007).

52. V. Vestreng, G. Myhre, H. Fagerli, S. Reis, and L. Tarrasón, "Twenty-five years of continuous sulphur dioxide emission reduction in Europe," Atmos. Chem. Phys. Discuss. **7**, 5099–5143 (2007).

53. P. Chýlek, U. Lohmann, M. Dubey, M. Mishchenko, and R. Kahn, "Limits on climate sensitivity derived from recent satellite and surface observations," J. Geophys. Res., submitted (2007).

54. E. I. Terez and G. A. Terez, "Investigation of atmospheric transmission in the Crimea (Ukraine) in the twentieth century," J. Appl. Meteorol. **41**, 1060–1063 (2002).

55. E. L. Makhotkina, I. N. Plakhina, and A. B. Lukin, "Some features of atmospheric turbidity change over the Russian territory in the last quarter of the 20th century," Russian Meteorol. Hydrol., No. 1, 20–27 (2005).

56. E. V. Gorbarenko, A. E. Erokhina, and A. B. Lukin, "Multiyear changes of aerosol optical thickness in Russia," Russian Meteorol. Hydrol., No. 1, 41–48 (2006).

57. C. Tomasi, V. Vitale, A. Lupi, C. Di Carmine, and M. Campanelli, "Aerosols in polar regions," J. Geophys. Res., in press (2007).

58. J. R. Norris and M. Wild, "Trends in aerosol radiative effects over Europe inferred from observed cloud cover, solar "dimming," and solar "brightening," J. Geophys. Res. **112**, D08214 (2007).

1. Introduction

Tropospheric aerosols are commonly believed to cause a significant forcing of climate via the direct and indirect radiative effects [1, 2]. However, the magnitude and potential variability of this forcing remain poorly constrained because of inadequate quantitative knowledge of global aerosol characteristics and their temporal changes ([3–6] and references therein). A number of active and passive satellite instruments have been used to retrieve global distributions of tropospheric aerosol properties [7–17]. While the newer instruments can be expected to provide more accurate aerosol retrievals, the older instruments, especially the Advanced Very High Resolution Radiometer (AVHRR) and the Total Ozone Mapping Spectrometer (TOMS), provide multidecadal information and can be used to assess potential long-term trends [18].

In a recent paper [19], we analyzed the Global Aerosol Climatology Project (GACP) dataset, which is based on AVHRR channel 1 and 2 radiances [8, 20–24], and identified a likely decrease of the global optical thickness of tropospheric aerosols by as much as 0.03 during the period 1991–2005. This potential trend mirrors the concurrent global increase in solar radiation fluxes at Earth's surface ([25–29] and references therein) and may have contributed to recent changes in surface temperature [30].

The objective of this companion paper is to evaluate the potential of long-term satellite remote sensing to reveal regional trends in the aerosol optical thickness (AOT) and size. A scrutiny of whether the derived trends are plausible or unrealistic can provide a valuable quality check on the GACP aerosol record. Indeed, the accuracy of GACP retrievals is

constrained by potential calibration uncertainties, which makes it rather difficult to identify weak long-term trends in the global aerosol load. However, long-term regional trends can be expected to be substantially stronger than those in the globally averaged AOT and thus should be easier to detect and quantify.

Consistent with this objective, we describe the most recent improvements made in the GACP retrieval algorithm, revisit the GACP record of the globally averaged AOT and Ångström exponent, and identify and discuss regional changes in the AOT and Ångström exponent that may have occurred between the three-year periods 1988–91 and 2002–05.

2. GACP retrieval algorithm

The GACP aerosol record [24] is derived from the International Satellite Cloud Climatology Project (ISCCP) DX radiance dataset composed of calibrated and sampled AVHRR radiances [31, 32]. Data from the following sun-synchronous polar-orbiting platforms have been included: NOAA-7 (August 1981 – January 1985), NOAA-9 (February 1985 – October 1988), NOAA-11 (November 1988 – September 1994), NOAA-14 (February 1995 – June 2001), and NOAA-16 (October 2001 – present). For a detailed discussion of the sampling resolution, calibration history, and changes in satellite sensors that enter the dataset we refer to [31–34].

The GACP algorithm yields the AOT and the Ångström exponent A for each cloud-free ISCCP pixel by minimizing the difference between two AVHRR radiances measured in the 0.65- and 0.85-μm channels at the specific illumination and observation angles determined by the satellite orbit, on the one hand, and the radiances computed theoretically for a realistic atmosphere–ocean model, on the other hand. The Ångström exponent is defined as

$$A = -\left.\frac{d[\ln C_{ext}(\lambda)]}{d(\ln\lambda)}\right|_{\lambda = \lambda_1}, \tag{1}$$

where $\lambda_1 = 0.65\,\mu$m is the nominal wavelength of the AVHRR channel 1 and C_{ext} is the ensemble-averaged extinction cross section per particle. The GACP aerosol product consists of the AOT reported at $\lambda = 0.55\,\mu$m and the constrained Ångström exponent [20]. It is limited to areas over large water bodies such as oceans, seas, and lakes, in which case the surface reflectance is often low and can be characterized with sufficient accuracy.

With only two radiance values per pixel available, the GACP retrieval algorithm cannot be expected to yield any additional parameters besides AOT and A and thus must rely on a number of assumptions which fix all other atmosphere and surface parameters globally and permanently. In particular, GACP retrievals are based on the assumption that aerosol particles are perfect spheres with a wavelength-independent refractive index $1.5 + i0.003$ and obey the following monomodal modified power law size distribution [8]:

$$n(r) = \begin{cases} C, & r \leq r_1, \\ C\left(\dfrac{r}{r_1}\right)^{-\alpha}, & r_1 < r \leq r_2, \\ 0, & r > r_2 \end{cases} \tag{2}$$

with $r_1 = 0.1\,\mu$m, $r_2 = 10\,\mu$m, and $\alpha \in [2.5, 5]$. The normalization constant C is chosen such that

$$\int_0^\infty dr\, n(r) = 1, \tag{3}$$

while the above range of power-exponent values translates into a representative range of A. The radiance contributions of the upwelling radiation from within the ocean body and of the white caps are modeled by assuming a small constant Lambertian component, while the

surface slope distribution is determined using the Cox–Munk relation and corresponds to a globally uniform wind speed value of 7 m/s. The single-scattering properties of the aerosol polydispersion are computed with a Lorenz–Mie code [35]. The multiple-scattering computations are performed using the scalar version of the adding–doubling technique [36]. The corresponding computer code incorporates the reflectance of the rough ocean surface via the modified Kirchhoff approximation [37] and the effect of water vapor, oxygen, and CO_2 absorption via the k-distribution technique [38]. For a complete description of the assumptions used in the algorithm and the cloud screening procedure we refer to [8, 20–23].

The two most recent modifications of the GACP retrieval algorithm have been as follows. First, we have extended the range of AOT values in the GACP look-up tables to 2.0 in order to account for rather frequent occurrences of large AOTs during dust and anthropogenic pollution outbreaks. Second, we have corrected for the effect of the slight Earth orbit eccentricity on the AVHRR radiances. The combined result of these modifications will be illustrated in the following section.

The GACP retrieval approach outlined above is consistent with the goal of minimizing long-term statistical errors in the global aerosol parameters derived by the algorithm. As such, it cannot preclude regional biases in areas dominated by aerosol types significantly different from the global model assumptions, for example, nonspherical dust and soot aerosols [21, 39, 40]. However, our present objective is to study long-term changes in the retrieved aerosol characteristics, and so we expect that the main conclusions drawn will hold despite potential systematic biases in the retrieved parameters.

3. Global averages

Figure 1 contrasts the global and hemispherical monthly averages of the AOT and Ångström exponent over the oceans for the period August 1981 – June 2005 derived with the old and the new version of the GACP retrieval algorithm. Note that two periods of unavailable or unreliable AVHRR data between July 1994 and February 1995 and between April (Janurary for the Ångström exponent) and August 2001 are excluded. For reference, the blue curve depicts the Stratospheric Aerosol and Gas Experiment (SAGE) record of the globally averaged stratospheric AOT. A specific analysis of the effects of stratospheric aerosols on GACP aerosol climatology and a detailed comparison of GACP and SAGE global aerosol records can be found in [22].

The two major AOT maxima in Fig. 1 are caused by the stratospheric aerosols generated by the El Chichon (March 1982) and Mt Pinatubo (June 1991) eruptions, whereas the quasi-periodic oscillations in the GACP curves are the result of inter-annual aerosol variability. One can identify specific discrepancies between the old and the new GACP results such as increased Northern-Hemisphere AOT values at the beginning of the El Chichon eruption. However, the average differences appear to be relatively small and rather insignificant.

The overall behavior of the GACP AOT during the quiescent period from January 1986 to June 1991 hardly reveals any statistically significant tendency. Namely, a linear model of the form $y = Ax + B$ fitted to the clear pre-Pinatubo period of data suggests that the global column AOT value just before the eruption was close to 0.144 according to the old retrieval algorithm and close to 0.145 according to the new algorithm. After the eruption, the GACP curves reveal complex tropospheric and stratospheric AOT temporal variations as well as a clear long-term decreasing trend in the tropospheric AOT [19]. To analyse the changes during this period, we calculated a linear fit of the form $y = Cx + D$ using data from January 1996 to June 2005 such that its extrapolation back to June 1991 gave us the previously found clear-period AOT value. This two-step procedure allowed us to exclude from the tendency analysis the period affected by the Pinatubo eruption. As a result, we found that the residual decrease in the global tropospheric AOT during the 14-year period from June 1991 to June 2005 was close to 0.036 according to the old retrieval algorithm and close to 0.033 (~0.0024 per year) according to the new algorithm. For both fits, the corresponding chi-square values indicate that the fitted parameters are reliable at a very high confidence levels of over 99%.
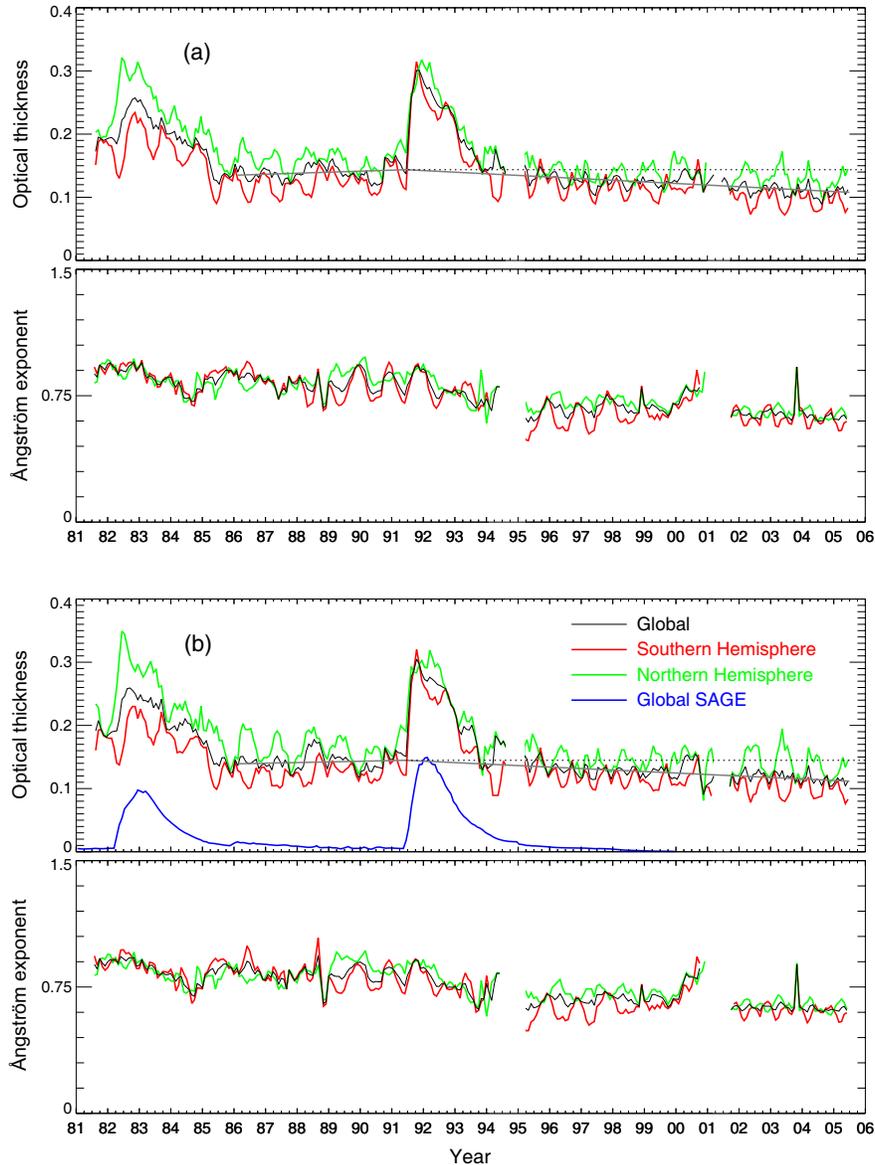
Fig. 1. Global and hemispherical monthly averages of the AOT and Ångström exponent over the oceans for the period August 1981 – June 2005 derived with (a) the old and (b) the new version of the GACP retrieval algorithm. The blue curve depicts the SAGE record of the globally averaged stratospheric AOT. The solid grey lines show pre- and post-Pinatubo linear regressions. The dotted grey line represnts the June 1991 pre-Pinatubo regression level.

Although there have been significant drifts in the equator crossing times for the individual AVHRR instruments [33, 34], Fig. 1 shows no obvious artifacts potentially attributable to the drifts. The only exception is the end of the NOAA-14 record when two factors caused the retrievals to be unreliable. First, the use of the pre-launch calibration of channel 2 radiances coupled with the likely strong degradation of the channel 2 sensitivity resulted in the spurious increase of the Ångström exponent. Second, the strong drift of the NOAA-14 orbit resulted in a partial loss of data and in a loss of coverage for much of the Southern Hemisphere, thereby causing a bias in the global and Southern-Hemisphere averages.

Overall, however, the GACP AOT record appears to be self-consistent, with no drastic intra-satellite variations, and is obviously consistent with the SAGE record. This seems to testify to the robustness of the ISCCP channel-1 radiance calibration and the GACP retrieval algorithm. This conclusion is reinforced by the close correspondence of the calculated and observed top-of-the-atmosphere solar fluxes [41]. Furthermore, GACP AOT retrievals have been successfully validated against precise sun-photometer data taken from 1983 through 2004 by employing a special procedure which, by design, tested the entire retrieval process as well as the radiance calibration [42, 43].

According to Fig. 1, the Ångström exponent appears to have decreased by about 0.3 over the duration of the GACP record. However, the retrieval accuracy for A is expected to be worse than that for τ because the central wavelengths of AVHRR channels l and 2 are rather close [8]. In addition, the Ångström exponent retrieval often "saturates" by yielding a value equal to either the upper or the lower boundary of the A range afforded by the nominal $\alpha \in [2.5, 5]$ range of power exponent values in Eq. (2) [20]. Such retrievals are not included in the computation of monthly averages, which reduces the number of useful data points and the accuracy of the final result. Furthermore, the accuracy with which A is retrieved depends on the relative calibration of channel-1 and -2 radiances. Since we use the ISCCP calibration of channel-1 radiances and the NOAA calibration of channel-2 radiances, additional studies may be necessary before the decreasing Ångström exponent trend is accepted as a definitive result (cf. [18, 22]).

4. Regional aerosol trends

The visualization of potential long-term regional aerosol trends is not as straightforward as that of the global averages because of the much larger amount of data to be displayed. The approach adopted for this study has been to plot three-year averages computed for two quiescent, volcano-free periods: the one preceding the Mt Pinatubo eruption and the one covering the most recent period of the GACP record. The results computed for the cumulative annual 1°×1° averages and for four seasonal 1°×1° averages are depicted in Figs. 2–7.

The accuracy and reliability of each 1°×1° average in Figs. 2–7 depends on the number of daily values contributing to the average. In addition, given the range of natural aerosol variability, the values for individual pixels may have been affected by local events such as fires, dust storms, and changes in atmospheric circulation and local conditions. To reveal the cause of the changes in a particular small area and to decide whether they are realistic or not would require a tedious case-by-case pixel-level analysis, which is far beyond the scope of this paper. We, therefore, chose not to segregate the reported 1°×1° averages based on the corresponding numbers of contributing daily values. Instead we concentrate on global and large-scale regional changes that these figures reveal. One should, nonetheless, bear in mind that aerosol retrievals in the narrow coastal zones may often pose a problem and may result in spurious features caused by a statistically insufficient number of daily retrievals used to compute an average value. A potential manifestation of this boundary effect may be seen along the western coast of Portugal in Fig. 2(c), thereby indicating that some of the coastal results in Figs. 2–7 may require critical re-evaluation.

The bottom panels in Figs. 2–6 demonstrate pronounced regional AOT changes that appear to have occurred between the late 1980s–early 1990s and the early 2000s. Although there is a significant seasonal variability in these changes, the most obvious regional AOT trends can be summarized as follows:

- a significant decrease over much of Europe and especially over the Black Sea (cf. [23]);
- a significant decrease over the part of the Atlantic Ocean most affected by dust aerosols originating in Africa;
- a noticeable increase along the part of the western coast of Africa most affected by biomass burning events; however, this trend appears to have strong seasonality and is even replaced by a decreasing tendency during the autumn;
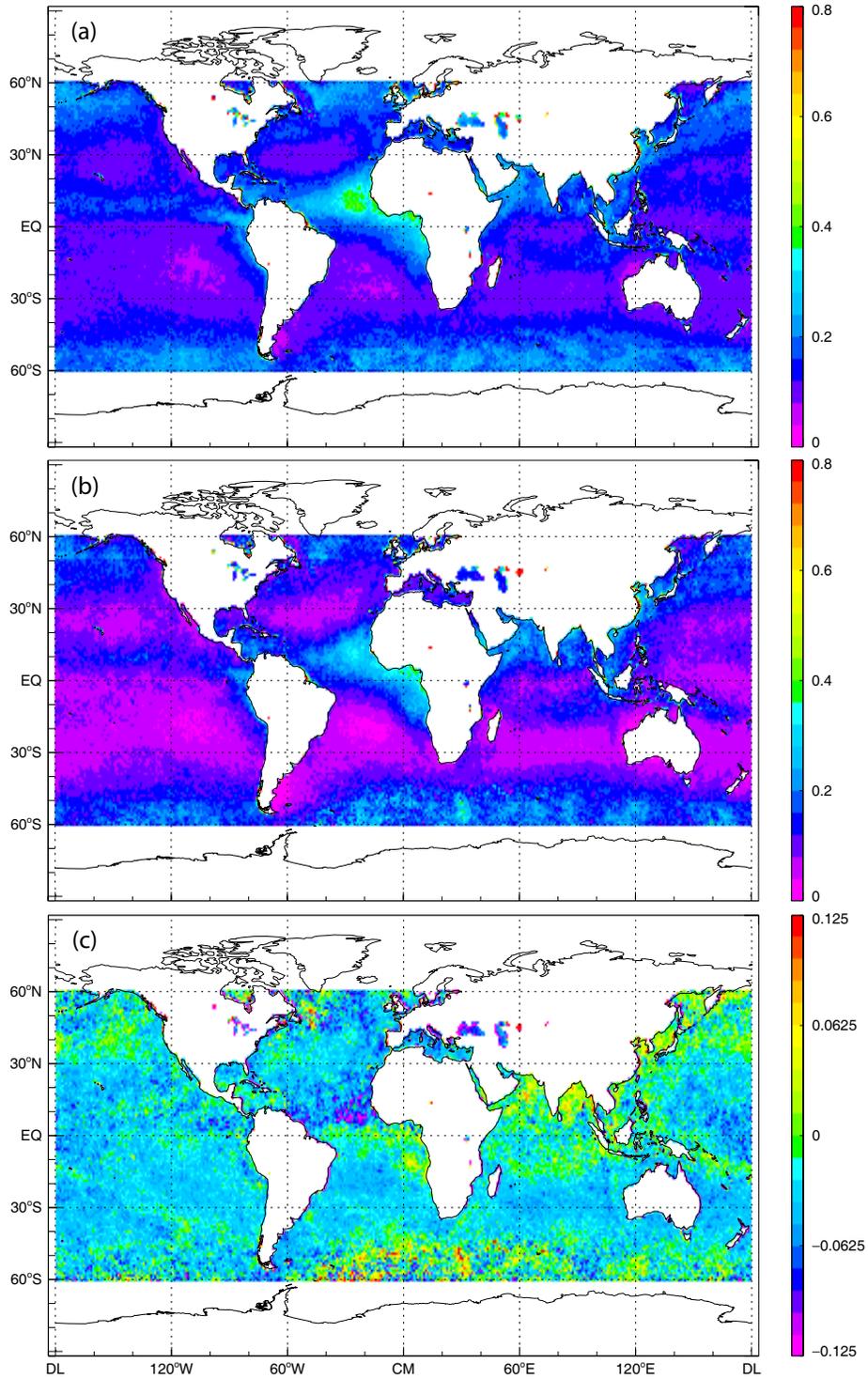
Fig. 2. (a) AOT averaged over the period July 1988 – June 1991. (b) AOT averaged over the period July 2002 – June 2005. (c) Difference between the AOT averages in panels (b) and (a).
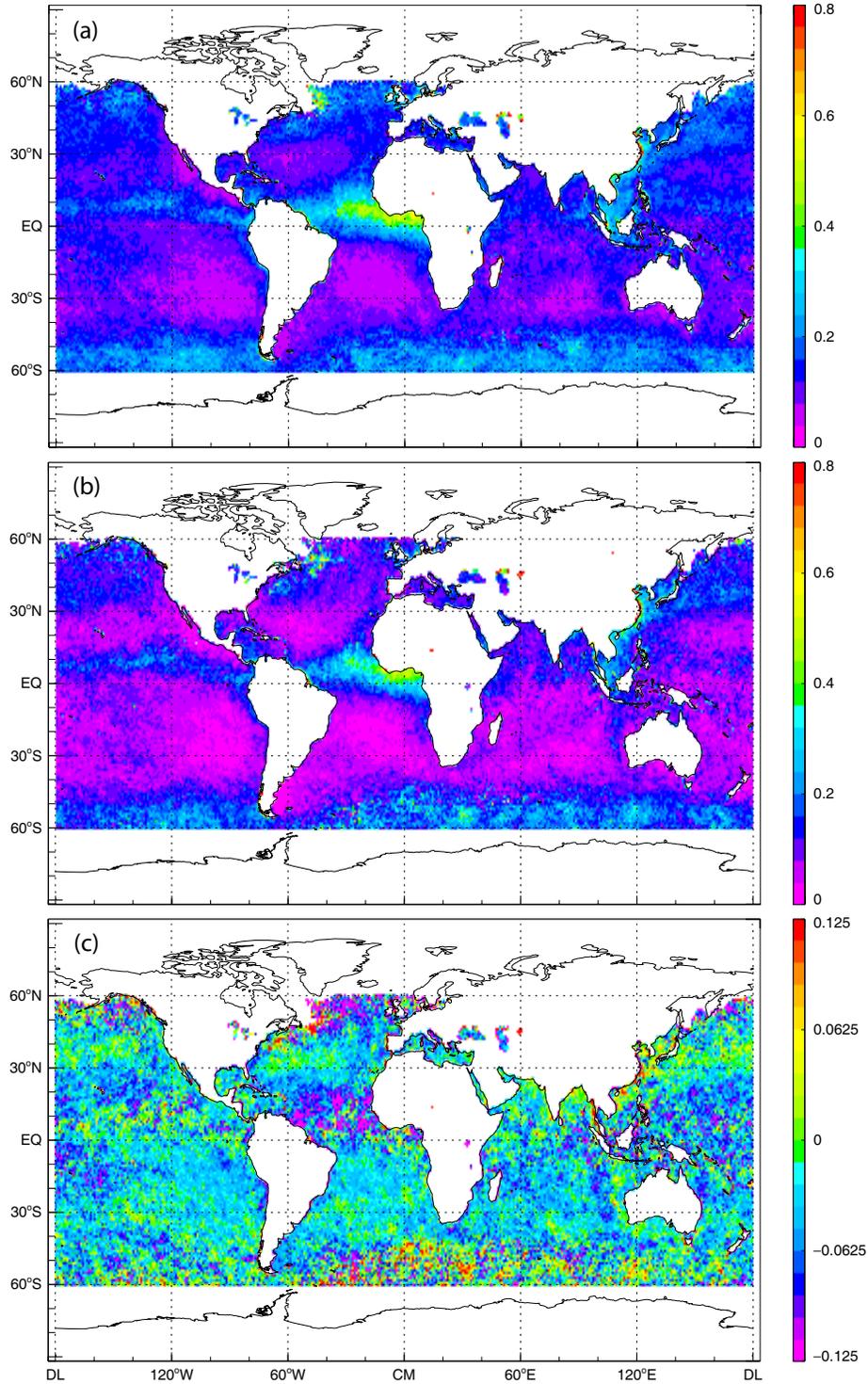
Fig. 3. (a) AOT averaged over the months December, January, and February in 1989–1991. (b) AOT averaged over the months December, January, and February in 2003–2005. (c) Difference between the AOT averages in panels (b) and (a).
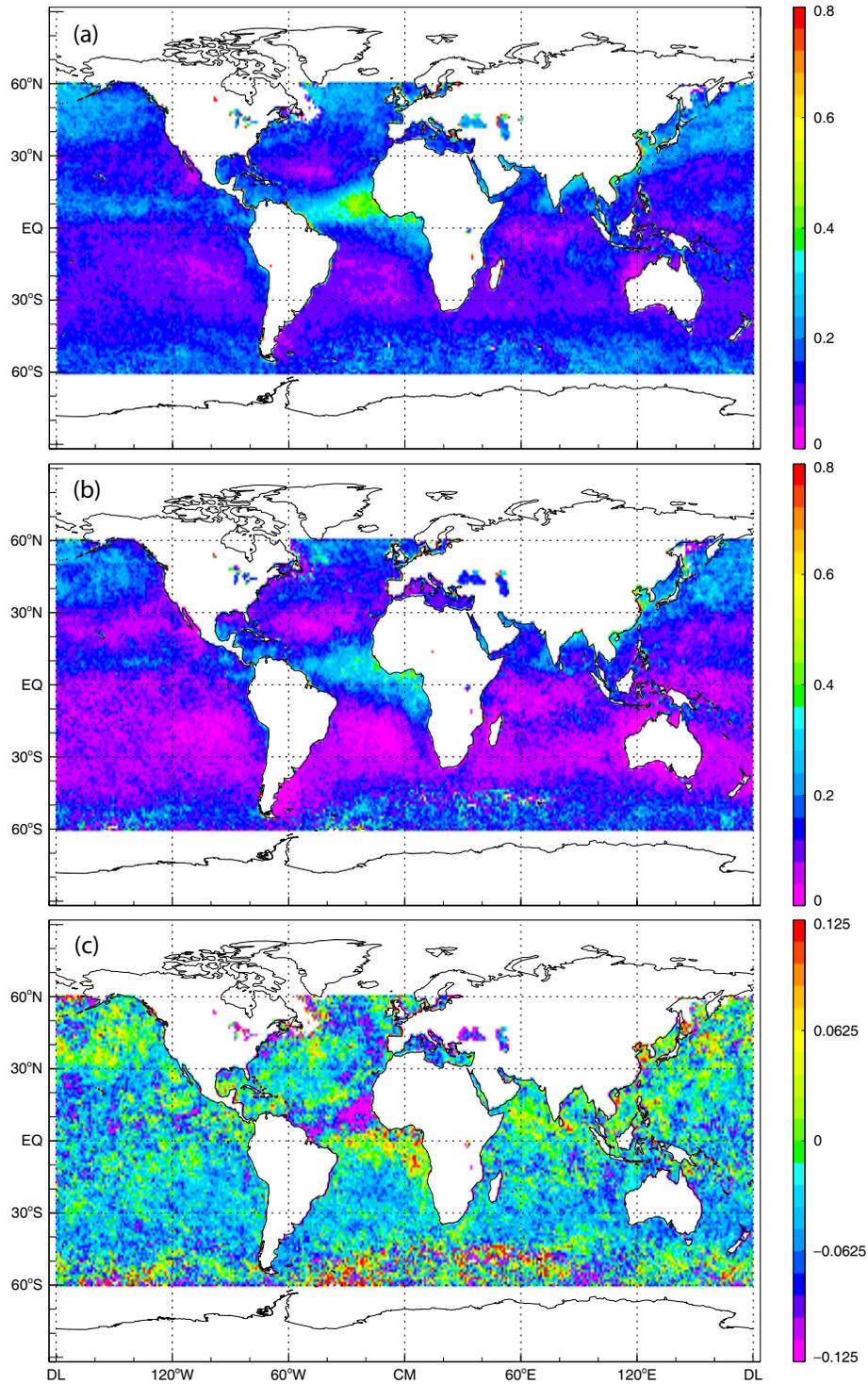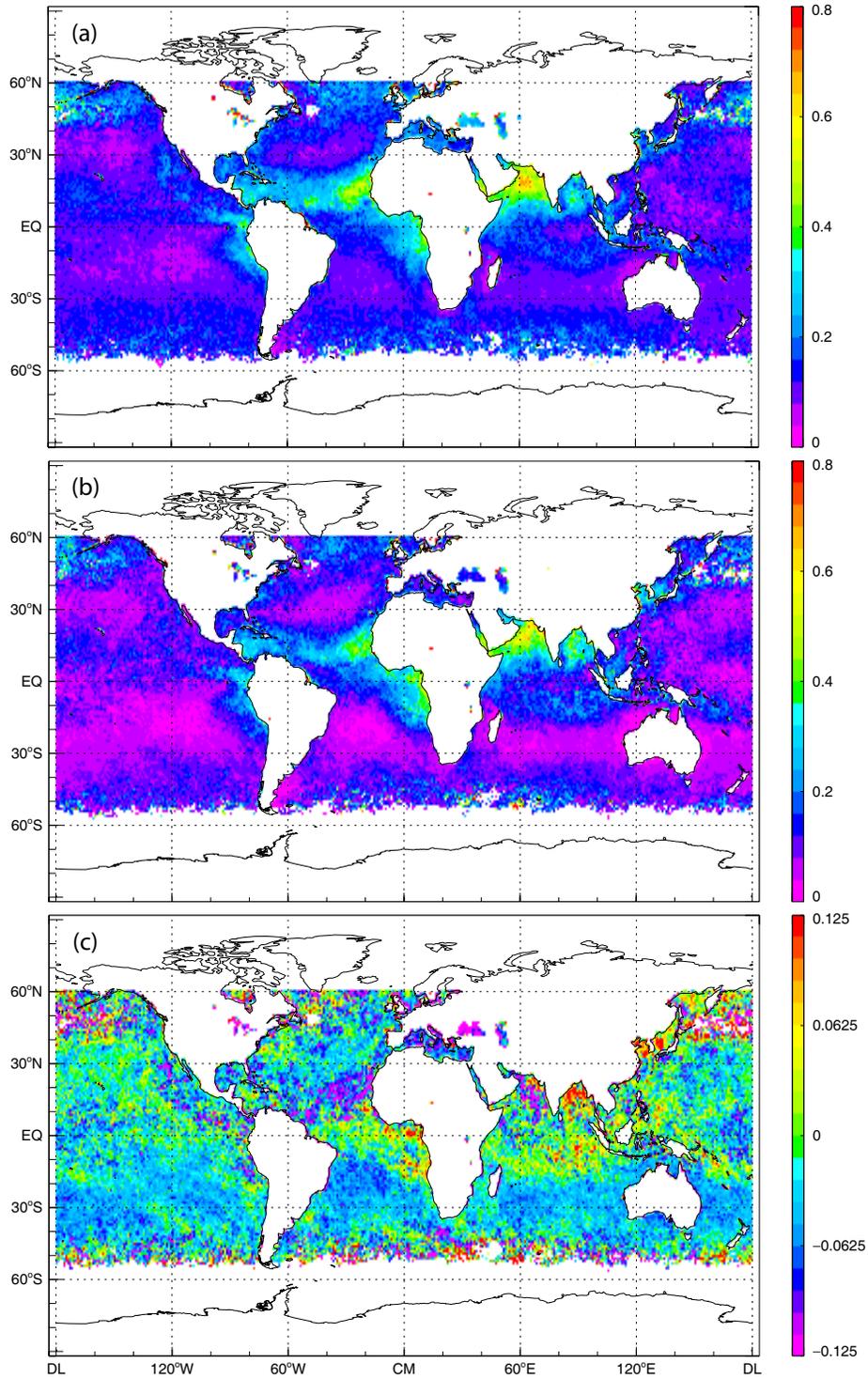
Fig. 4. (a) AOT averaged over the months March, April, and May in 1989–1991. (b) AOT averaged over the months March, April, and May in 2003–2005. (c) Difference between the AOT averages in panels (b) and (a).

Fig. 5. (a) AOT averaged over the months June (1989–1991), July (1988–1990), and August (1988–1990). (b) AOT averaged over the months June (2003–2005), July (2002–2004), and August (2002–2004). (c) Difference between the AOT averages in panels (b) and (a).
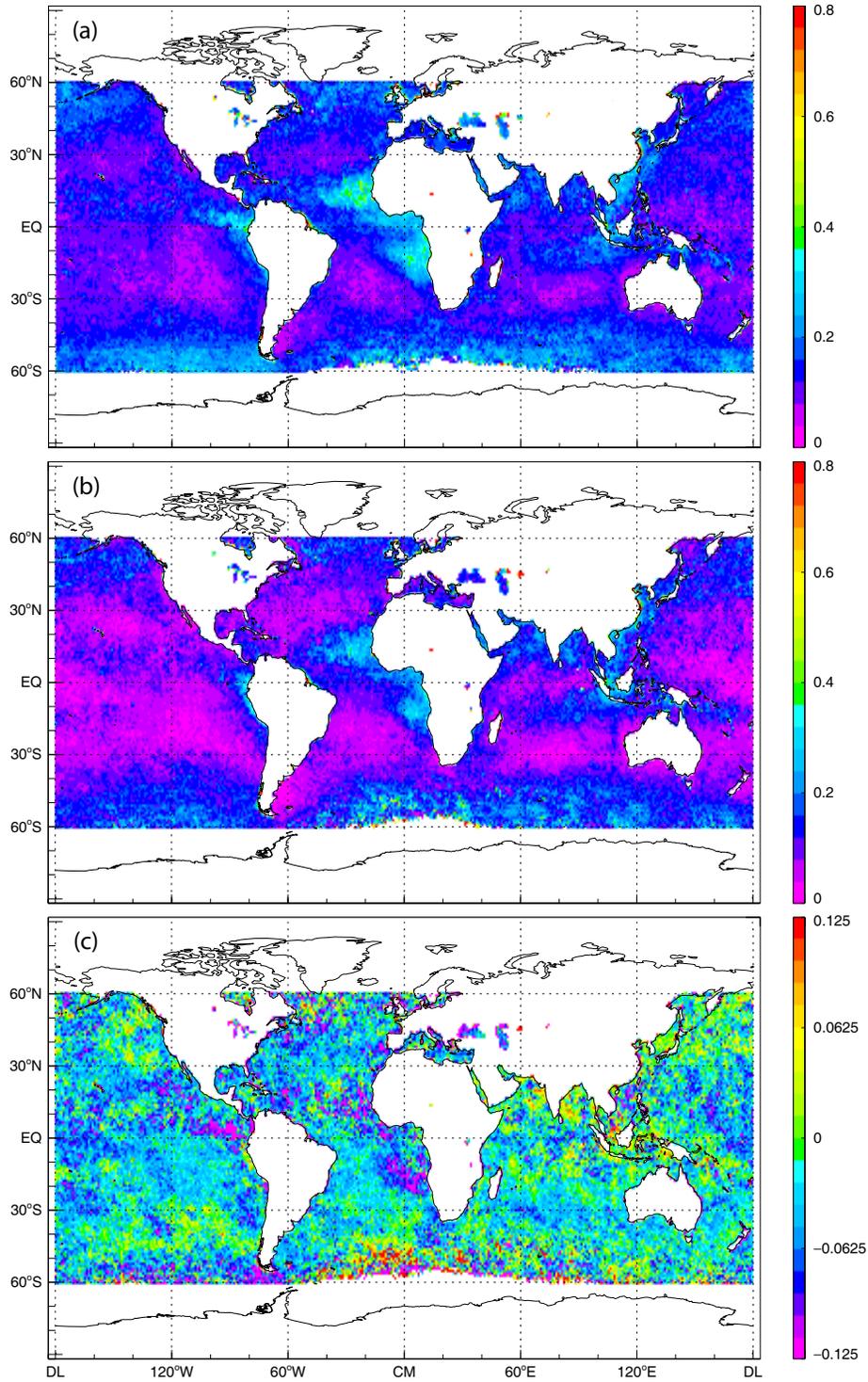
Fig. 6. (a) AOT averaged over the months September, October, and November in 1988–1990. (b) AOT averaged over the months September, October, and November in 2002–2004. (c) Difference between the AOT averages in panels (b) and (a).
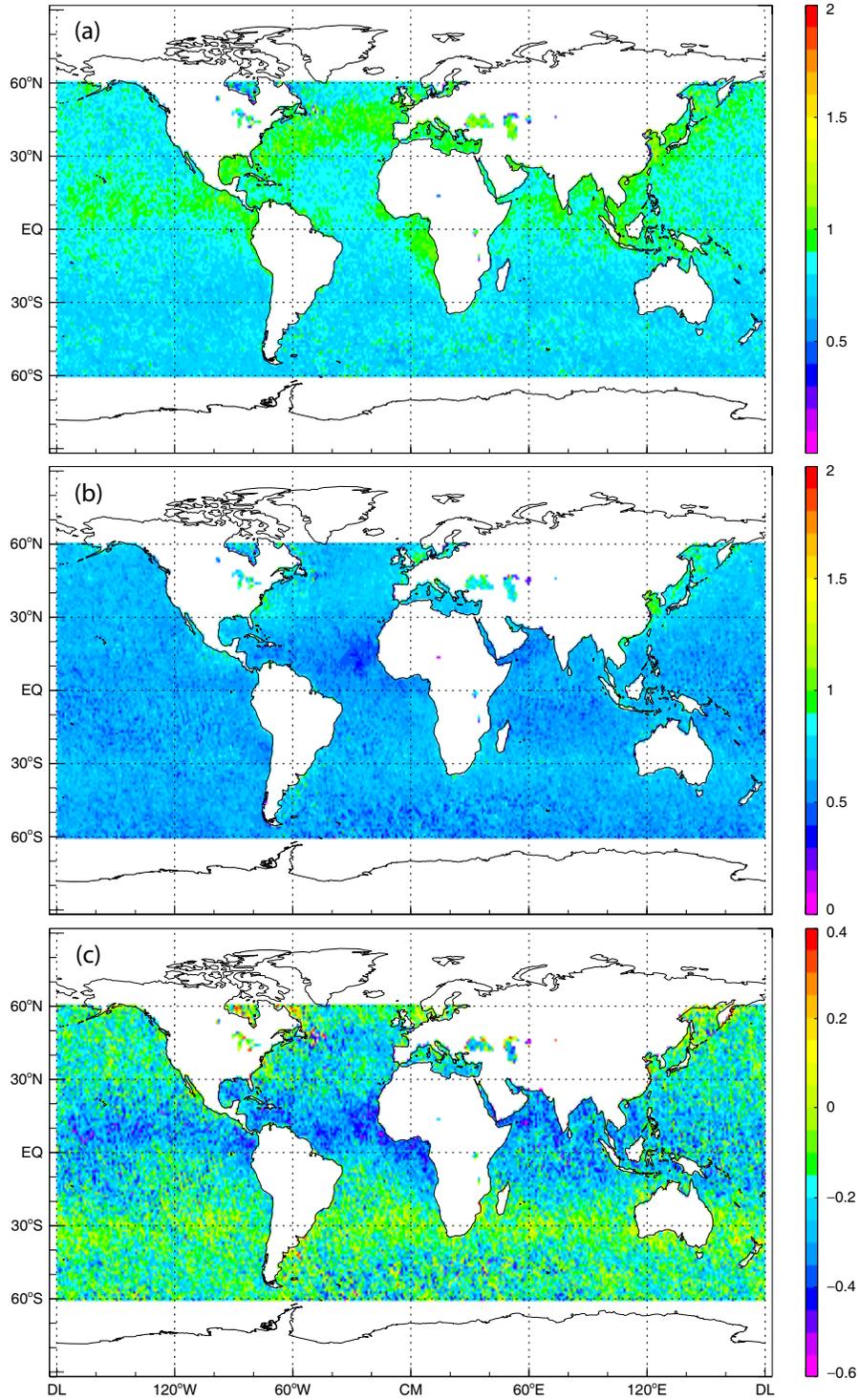
Fig. 7. (a) Ångström exponent averaged over the period July 1988 – June 1991. (b) Ångström exponent averaged over the period July 2002 – June 2005. (c) Difference between the Ångström exponent averages in panels (b) and (a).

- a significant increase along the southern and south-east coasts of Asia, especially for the summer months; and
- a significant increase over the 45°S–60°S latitudinal belt.

These regional trends appear to be superposed on a fairly uniform global decrease of AOT causing the downward trend in the global and hemispheric AOT averages in Fig. 1.

Figure 7(c) also reveals noticeable regional changes in the Ångström exponent:

- a significant decrease over the areas of the Atlantic Ocean affected by the African dust and biomass burning aerosols;
- a substantial decrease over the Northern and Central Indian Ocean;
- a significant decrease over the equatorial part of the Pacific Ocean; and
- a noticeable increase over the 15°S–45°S latitudinal belt.

5. Discussion

Not being experts in the subject area of aerosol production, processing, and transport, we may not be able to explain or evaluate the plausibility of all the features of the aerosol global distribution and its seasonal and decadal variability supposedly revealed by Figs. 2–7. In this respect, Figs. 2–7 are intended to inform the aerosol community at large of new and potentially important information worthy of a detailed critical analysis. The purpose of the following discussion is to provide a limited assessment consistent with our own knowledge and understanding.

The strong AOT decrease over the large Atlantic Ocean area between the equator and 30°N appears to indicate a reduced productivity of the African sources of dust aerosols. This finding is perfectly consistent with the results of [44, 45] indicating that the amount of rain and vegetation in the Sahel has increased significantly since the late 1980s. An alternative or an additional explanation may be that the dust particles have become larger and, as a result, spend less time in the atmosphere. The latter explanation would be consistent with the concurrent decrease of the Ångström exponent in this area, Fig. 7(c). An interesting feature of Figs. 3–6 is that the overall seasonal morphology of the dust plume has hardly changed despite the significant decrease in the total amount of dust.

The overall AOT increase along the western coast of Africa from the equator to about 20°S may be explained by intensified biomass burning. We have mentioned, however, that this overall increasing trend appears to be replaced by a decreasing trend during the autumn months, as Fig. 6(c) indicates. The significant inter-annual variability of the AOT in this region perfectly correlates with expected changes in the number and extent of fires during the local dry and rainy seasons.

The noticeable AOT increase along the southern and south-east coasts of Asia can be the expected result of rapidly growing regional economies coupled with the widespread use of technologies that are not environmentally clean [46–48].

The elevated amounts of aerosols throughout the 40°S–60°S latitudinal belt, Figs. 2(a) and 2(b), correlate almost perfectly with the Special Sensor Microwave/Imager (SSM/I) [49] surface wind speed data, Figs. 8(a) and 8(b). It is well known that increasing wind speed can lead to increased sea-salt aerosol production [50] as well as cause increased ocean surface reflectivity by both making the ocean surface more rough and generating more white caps. Since the GACP retrieval algorithm is based on a constant wind speed value and a constant diffuse component of the ocean surface reflectance, all of these factors would have the same effect on the GACP-derived AOT, thereby potentially making a part of it artificial. It is interesting that even the long-term AOT increase in this area seen in Fig. 2(c) may correlate with the contemporaneous wind speed increase revealed by Fig. 8(c). Partial cloud contamination of "clear-sky" pixels used for aerosol retrievals is also a constant concern in this cloud-dominated region. Obviously, this remote area of the globe represents a challenging problem in terms of aerosol retrievals; the solution of this problem may require much more capable satellite instruments such as the Aerosol Polarimetry Sensor [51] or even
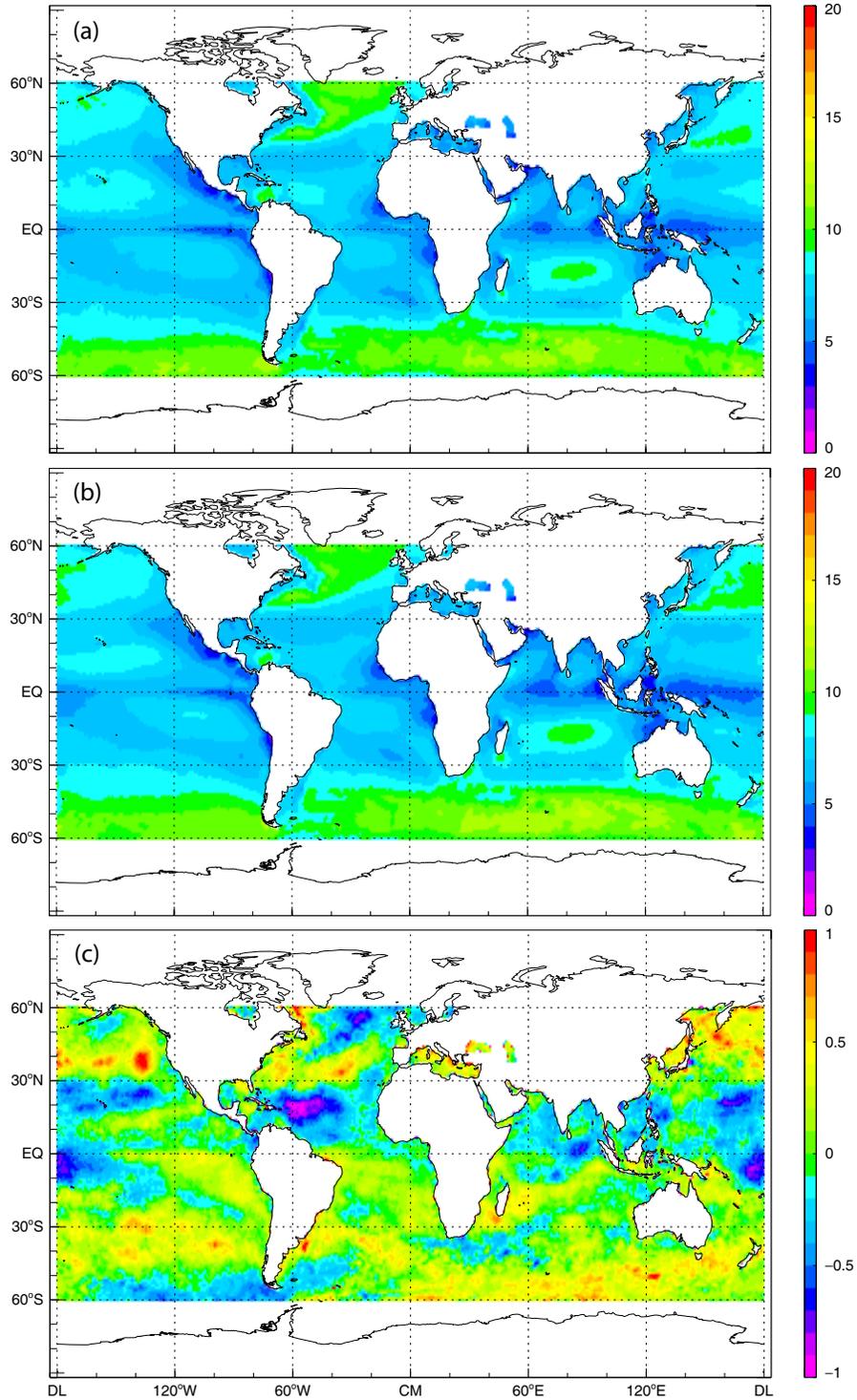
Fig. 8. (a) Surface wind speed averaged over the period July 1988 – June 1991. (b) Surface wind speed averaged over the period July 2002 – June 2005. (c) Difference between the surface wind speed averages in panels (b) and (a).

a combination of passive and active sensors.

The significant long-term AOT decrease over much of Europe is quite consistent with the supposed reversal from increasing to decreasing anthropogenic sulfur and black carbon emissions owing to the enactment of clean air legislation in many countries [46, 47, 52]. The enactment of similar legislation in the USA may have led to a similar decrease of AOT over much of the US territory [53] not necessarily revealed by the GACP data. The downfall of the local economies throughout the territory of the former Soviet Union had also resulted in a dramatic and well documented decrease of aerosol emissions and AOT [23, 54–56]. These three factors, coupled with long-range aerosol transport, may have had a significant global impact, potentially causing much of the long-term AOT trend revealed by Fig. 1.

6. Conclusion

Based on the above limited discussion, we conclude that the long-term regional AOT trends revealed by Figs. 2–6 appear to be generally plausible. They are qualitatively consistent with both the results of extensive ground-based observations [23, 54–57] and the recent emission-inventory assessments [46–48, 52]. To the extent that radiance calibration remains to be a potentially significant source of uncertainty, our regional results cannot prove unequivocally the existence of the relatively weak downward trend in the global and hemispherical AOT averages. However, their plausibility appears to increase the trustworthiness of the overall trend. An additional, albeit indirect, confirmation of the overall decreasing tendency in AOT comes from the widespread contemporaneous reversal from global solar dimming to global solar brightening [25, 27–29, 58].

We thus believe that the totality of our results demonstrates the potential of satellite remote sensing to identify long-term aerosol trends. Nevertheless, more work still needs to be done in terms of both verification and potential improvement of the AVHRR radiance calibration and comparisons of GACP aerosols retrievals with potentially more accurate retrievals afforded by the newer satellite instruments [18].

Acknowledgments